A01-16491

AIAA 2001-0635

Large-Eddy Simulation of Fuel-Air Mixing in an Internal Combustion Engine

Kazuo Sone, Nayan Patel and Suresh Menon
School of Aerospace Engineering
Georgia Institute of Technology
Atlanta, Georgia 30332-0150

39th AIAA Aerospace Sciences Meeting
January 8–11, 2001 / Reno, NV

Large-Eddy Simulation of Fuel-Air Mixing in an Internal Combustion Engine

Kazuo Sone*, Nayan Patel† and Suresh Menon‡
School of Aerospace Engineering
Georgia Institute of Technology
Atlanta, Georgia 30332-0150

In this study, a Large-Eddy Simulation (LES) methodology has been implemented into the well-known Internal Combustion (IC) engine simulation code KIVA-3V and used to study unsteady fuel-air mixing process in a Direct-Injection Spark-Ignition type IC engine. This new code incorporates a LES approach (called henceforth KIVALES) using the k-equation SGS model (Menon *et al.*, 1996) and a modified version of the Linear-Eddy Mixing (LEM) model. To evaluate the accuracy of KIVALES, comparisons between KIVALES, original KIVA-3V, and another high-order LES code (well-validated elsewhere) are first carried out using flow over backward-facing step and temporally growing mixing layers. These types of flows are well known and therefore, sufficient data is available for comparison. Good agreement is obtained with earlier DNS/LES or experimental study using the new KIVALES, whereas the original KIVA-3V shows poor agreement. Next, both KIVALES and KIVA-3V are used to study fuel-air mixing process with direct spray injection into the cylinder. The comparisons between KIVALES with and without LEM and the original KIVA-3V are also made. A qualitative comparison (since no experimental data is available) suggests that KIVALES predicts significantly more unsteady mixing regions than KIVA-3V. The implications of the non-homogeneous mixed region on combustion are discussed.

1 Introduction

Recent progress in spray combustion has made it possible to produce direct injection gasoline engine that is expected to have advantages of both conventional diesel and gasoline engines. Since current port fuel injection type gasoline engine is at the state-of-the-art and is less likely to experience great progresses in the next decade, gasoline direct injection technology is a promising technology, capable of achieving very severe emission standards and restrictions such as EURO IV or SULEV. The critical issue associated with direct injection engine or even other types of spray combustion system is that we have to understand the liquid fuel evaporation process and the subsequent mixing of the vaporized fuel with air in the cylinder. This process is very sensitive to the type of fuel injectors, its operating parameters and so on, and it is apparent that the successful control of spray dispersion and turbulent fuel-air mixing process will imply an efficient direct injection engine.

To achieve this goal, the efficient use of computational tools is inevitable since the in-cylinder flow field with spray is quite hard to visualize or to measure accurately even with up-to-date experimental techniques. Numerical studies of direct injection engine has been carried out by many authors,[1,2] and they are comprehensively reviewed by Zhao.[3] However, most of the Internal Combustion engine simulations are performed using Reynolds-Averaged Navier-Stokes (RANS) equations with turbulence model such as the well known $k-\varepsilon$ model, which the KIVA code[4] used in this study, also employs. It is recognized, however, that steady-state models do not have the ability to capture unsteady mixing process inside the cylinder accurately since all turbulence effects are modeled (therefore, the model is also called a full-field model[5]). There is another technique called Large-Eddy Simulation (LES), in which larger eddies are calculated explicitly in a space- and time-accurate manner while smaller eddies that are of the scale of the computational grid or smaller are modeled using subgrid scale (SGS) models. Application of LES to IC engines is relatively new and less common while application of LES in other flow fields is rapidly growing.[6] LES studies of IC engine flows have been recently reported by several authors.[7-9]

*Graduate Research Assistant, Student Member AIAA; Current address, Hitachi America, Ltd., R & D Division, 34500 Grand River Avenue, Farmington Hills, MI 48335
†Undergraduate Research Assistant, Student Member AIAA
‡Professor, Associate Fellow AIAA

A recent attempt by Celik *et al.*[10] actually implemented LES models into an earlier version of the KIVA code. Nearly all these earlier LES attempts employed the Smagorinsky's algebraic eddy viscosity SGS model and no study so far has addressed subgrid scalar mixing.

Here, LES with well-validated k-equation SGS model[11] is implemented into the most recent commercial IC engine simulation code (KIVA-3V), which originally solves the RANS equations with the $k-\varepsilon$ model. The new code is denoted here as KIVALES, and the accuracy of the code is evaluated with the simulations of temporal mixing layer and flow over rearward-facing step. The new code is, then, applied to direct injection engine simulations to study spray dispersion and fuel-air mixing process associated with fuel spray evaporation.

To investigate scalar mixing at the small scales, a subgrid scalar mixing model called the Linear-Eddy Mixing (LEM) model is also implemented. LEM was originally developed by Kerstein[12] for stand-alone turbulent mixing, but later, it was found to be effective as a SGS scalar mixing model for LES.[13] LEM is particularly attractive for turbulent reacting flows since all the relevant scales are resolved in a 1-D LEM domain inside each LES computational cell. Thus, the reaction-rate and molecular diffusion effects can be computed in an exact manner without requiring any closure model.

2 Governing Equations

The conservative equations for compressible flow are filtered with a density-weighted box filter to obtain equations for LES, and they are described as follows.

$$\frac{\partial \bar{\rho}}{\partial t}+\frac{\partial \bar{\rho}\widetilde{u}_j}{\partial x_j}=\overline{\dot{\rho}^s} \tag{1}$$

$$\frac{\partial \bar{\rho}\widetilde{u}_i}{\partial t}+\frac{\partial}{\partial x_j}\left(\bar{\rho}\widetilde{u}_i\widetilde{u}_j-\bar{\tau}_{ij}+\tau_{ij}^{sgs}\right)=\overline{F_i^s} \tag{2}$$

$$\begin{aligned}&\frac{\partial \bar{\rho}\widetilde{e}}{\partial t}+\frac{\partial}{\partial x_j}\left(\bar{\rho}\widetilde{u}_j\widetilde{e}+\bar{q}_j+h_j^{sgs}\right)\\&=-\bar{p}\frac{\partial \widetilde{u}_j}{\partial x_j}+\overline{\sigma}_{ij}\frac{\partial \widetilde{u}_i}{\partial x_j}+\Theta^{sgs}+\Pi^{sgs}+\overline{\dot{Q}^s}\end{aligned} \tag{3}$$

$$\frac{\partial \bar{\rho}\widetilde{Y}_m}{\partial t}+\frac{\partial}{\partial x_j}\left(\bar{\rho}\widetilde{u}_j\widetilde{Y}_m-\bar{\rho}\bar{D}_m\frac{\partial \widetilde{Y}_m}{\partial x_j}+\Phi_{j,m}^{sgs}+\theta_{j,m}^{sgs}\right)=\overline{\dot{\rho}_m^s}, \tag{4}$$

where stress tensor $\tau_{ij}=-p\delta_{ij}+\sigma_{ij}=-p\delta_{ij}+2\mu(S_{ij}-1/3S_{kk}\delta_{ij})$, and heat flux $q_j=-\kappa\partial T/\partial x_j+\rho\sum_{m=1}^{N}h_mY_mV_{j,m}$. Throughout this study, Fickian diffusion is used to model species diffusion velocity $V_{j,m}$.

Following original KIVA code, we employ the specific internal energy equation rather than the total energy equation.[14] To the authors' best knowledge, specific energy equation has never been published elsewhere in a context of LES except by Celik *et al.* However, in that work, the details of the closure of specific internal energy equation was not described. Therefore, for completeness we describe the derivation and filtering of the internal energy equation in the Appendix.

In the above equations, the following subgrid related terms are unclosed and have to be modeled:

$$\tau_{ij}^{sgs} = \bar{\rho}[\widetilde{u_iu_j}-\widetilde{u}_i\widetilde{u}_j], \tag{5}$$

$$h_i^{sgs} = \bar{\rho}[\widetilde{eu_i}-\widetilde{e}\widetilde{u}_i]+[\overline{pu_i}-\bar{p}\widetilde{u}_i], \tag{6}$$

$$\Theta^{sgs} = \overline{\sigma_{ij}\frac{\partial u_i}{\partial x_j}}-\overline{\sigma}_{ij}\frac{\partial \widetilde{u}_i}{\partial x_j}, \tag{7}$$

$$\Pi^{sgs} = \overline{u_j\frac{\partial p}{\partial x_j}}-\widetilde{u}_j\frac{\partial \bar{p}}{\partial x_j}, \tag{8}$$

$$\Phi_{i,m}^{sgs} = \bar{\rho}[\widetilde{u_iY_m}-\widetilde{u}_i\widetilde{Y}_m], \text{ and} \tag{9}$$

$$\theta_{i,m}^{sgs} = \bar{\rho}[\widetilde{V_{i,m}Y_m}-\widetilde{V}_{i,m}\widetilde{Y}_m]. \tag{10}$$

These terms represent subgrid stress tensor, subgrid heat flux, subgrid viscous work, subgrid velocity pressure gradient correlation, subgrid species mass flux and diffusive mass flux, respectively. The closure of these terms are considered in the following section.

3 Subgrid Modeling

The small scale effects on a resolved scale is approximated by SGS models in LES. Even though LES is less model dependent than RANS, the selection of SGS models is of great importance and a challenging part of research in LES. In this study, k-equation model developed by Menon *et al.*[11] is adopted. In this model, subgrid stress tensor τ_{ij}^{sgs} is modeled as $\tau_{ij}^{sgs}=-2\bar{\rho}\nu_t(\widetilde{S}_{ij}-(1/3)\widetilde{S}_{kk}\delta_{ij})+(2/3)\bar{\rho}k^{sgs}\delta_{ij}$, with eddy viscosity given by $\nu_t=C_\nu k^{sgs\,1/2}\overline{\Delta}$ using subgrid turbulent kinetic energy k^{sgs}, which is provided by solving the following equation.

$$\frac{\partial \bar{\rho}k^{sgs}}{\partial t}+\frac{\partial \bar{\rho}\widetilde{u}_jk^{sgs}}{\partial x_j}=P^{sgs}-D^{sgs}+T^{sgs}+\dot{W}^s, \tag{11}$$

where the production term, P^{sgs} is closed by $-\tau_{ij}^{sgs}(\partial\widetilde{u}_i/\partial x_j)$, and the subgrid energy dissipation rate term D^{sgs} is closed by $C_\varepsilon\bar{\rho}k^{sgs\,3/2}/\overline{\Delta}$. The transport term $T^{sgs}=\nabla\cdot\{(\bar{\rho}\nu_t/Pr_t)\nabla k^{sgs}\}$. For the

present study, C_ν and C_ε are constant and chosen as 0.067 and 0.916, respectively.[15] A more expensive dynamics version is also available,[16,17] but is not used at present. The last term $\dot{W}^s$ is the subgrid turbulence effects due to spray, and this term follows the original KIVA model.[14]

The species mass flux Φ^{sgs} is modeled by gradient diffusion closure,

$$\Phi^{sgs}_{i,m} = -\bar{\rho}\frac{\nu_t}{Sc_t}\frac{\partial \widetilde{Y_m}}{\partial x_i}, \tag{12}$$

in the conventional approach and the present study also uses this closure (KIVALES). The diffusive mass flux $\theta^{sgs}_{i,m}$ is ignored in this study since this term is small compared to $\Phi^{sgs}_{i,m}$.[18]

The velocity pressure gradient correlation term Π^{sgs} is ignored, and h^{sgs}_j term is modeled by gradient diffusion $h^{sgs}_j = -\bar{\rho}\nu_t C_p/Pr_t(\partial\widetilde{T}/\partial x_j)$, by the analogy from H^{sgs} term closure.[18] Finally, Θ^{sgs} stands for subgrid viscous work, and following original KIVA-3V, is modeled by SGS turbulent energy dissipation rate $\Theta^{sgs} = D^{sgs} = C_\varepsilon \bar{\rho} k^{sgs\,3/2}/\overline{\Delta}$. This term has been neglected in the earlier LES studies.[18,19] The implications of this term in terms of SGS model is discussed elsewhere.[20]

4 Linear-Eddy Mixing Model

An alternate approach to study scalar mixing is based on the LEM model. In this model, the scalar conservation equations are not filtered. Instead, these scalar equations are implemented in a subgrid simulation model within the LES grid. This model was originally developed by Kerstein[12] for stand-alone simulation of turbulent mixing, and was extended into a subgrid model of LES.[13] LEM models subgrid scale mixing process in a one-dimensional computational domain within each LES cell. Therefore, each LES cell has a 1-D LEM domain within it and this 1-D domain is resolved with a grid fine enough to resolve the smallest turbulent eddy (e.g., Kolmogorov eddy). The key advantage of this model is that the two inherently different mixing processes, turbulent stirring and reaction-diffusion, can be treated separately but concurrently. Also, due to the 1-D nature of the LEM, the computational cost of subgrid simulation is also reasonable.

To implement LEM, the species conservation equation is re-written in the following form:

$$\frac{\partial Y_m}{\partial t} + (\widetilde{u}_j + u''_j)\frac{\partial Y_m}{\partial x_j} - \frac{1}{\rho}\frac{\partial}{\partial x_j}\rho D_m \frac{\partial Y_m}{\partial x_j} = 0, \tag{13}$$

where $\tilde{u}_j$ is the Favre-filtered velocity and $u''_j = u_j - \tilde{u}_j$ is unresolved velocity. Note that this equation is not filtered unlike Eqn.(4). Therefore, no additional closure is required. This equation is solved in three phases employed in KIVA as follows:

$$\frac{Y^B_m - Y^n_m}{\Delta t} = \frac{1}{\rho}\frac{\partial}{\partial x_j}\rho D_m \frac{\partial Y_m}{\partial x_j} - u'_j \frac{\partial Y_m}{\partial x_j} \tag{14}$$

$$\frac{Y^{n+1}_m - Y^B_m}{\Delta t} = -\left(\widetilde{u}_j + u'_j\right)\frac{\partial Y_m}{\partial x_j}. \tag{15}$$

Superscripts n, A, B denote respectively time level, phase A, in which spray and chemistry is solved, and phase B, in which Lagrangian fluid motions are solved.[14] At present, we have not implemented subgrid combustion, but this extension can be accomplished within LEM subgrid model. Equation (15) is solved on the resolved scale while equation (14) is implemented in the 1-D LEM domain in the following form.

$$\frac{\partial Y_m}{\partial t} = \frac{1}{\rho}\frac{\partial}{\partial s}\rho D_m \frac{\partial Y_m}{\partial s} + F^{stir}_m, \tag{16}$$

where s is a coordinate along the LEM domain. In these equations, the molecular diffusion is implemented in the first term of the RHS and is solved explicitly as in a DNS while the subgrid scale advection (turbulent stirring) denoted as F^{stir}_m is modeled by a stochastic process. This is briefly discussed below, and more details can be found elsewhere.[13,15,21]

Turbulent stirring is implemented as random rearrangements of the scalar field along the 1-D domain. This random rearrangement physically represents eddy motion smaller than the computational grid size, $\overline{\Delta}$ and is governed by two parameters: a distribution of eddy size l in the subgrid domain $f(l) = (5/3)(l^{-8/3})/(\eta^{-5/3} - \overline{\Delta}^{-5/3})$ in the range $\eta < l < \overline{\Delta}$ and an event frequency per unit length Λ:[12]

$$\Lambda = \frac{54}{5}\frac{\nu Re^{sgs}}{\overline{\Delta}^3}\frac{\left(\overline{\Delta}/\eta\right)^{5/3} - 1}{1 - \left(\eta/\overline{\Delta}\right)^{4/3}}, \tag{17}$$

where subgrid Reynolds number is defined as $Re^{sgs} = u'\overline{\Delta}/\nu$, and $u' = \sqrt{(2/3)k^{sgs}}$. The assumption of statistical isotropy in 1-D domain is implemented by choosing the location of the events randomly from a uniform distribution. The random rearrangement events occur every stirring time interval. The stirring interval is given by $\Delta t_{stir} = 1/\Lambda\overline{\Delta}$, and in each event, segment that is affected by this random event is chosen according to the distribution described above and the rearrangement follows a triplet map procedure.[12]

To implement LEM into LES and to allow for advection of the subgrid scalar fields across LES cells

due to the large-scale resolved motion, a Lagrangian advection process is employed to model the process in equation (15). This concept suits ALE (Arbitrary Lagrangian-Eulerian) method, which is used in the KIVA code. In ALE method, Lagrangian phase and advection phase are treated respectively. There have been various attempts to address this issue.[18,19] In this study, linear superposition of subgrid field according to the local cell-face volume flux is implemented based on the recent work of Pannala[22] since this method suits phase C (advection phase) of KIVA. In this method, each upwind side subgrid scalar field is superimposed onto the adjacent downwind side subgrid field, and its ratio is determined by the local volume-flux ratio $(\mathbf{u} \cdot \mathbf{A}\Delta t/V)$.

5 Results and Discussion

5.1 Temporal Mixing Layer

First, the ability to simulate scalar mixing process of the new KIVALES code is examined using temporal mixing layers. The flow is initialized by a mean streamwise velocity with a tangent hyperbolic profile and with the fundamental instability mode with a non-dimensional wave number $\alpha = 0.446$, which is the most unstable wave number mode predicted by Michalke.[23] This initialization of velocity profile follows earlier DNS study by Metcalfe *et al.*[24] Another study by Riley and Metcalfe[25] showed that it takes a non-dimensional time of around 8 for the fundamental mode to grow and saturate. They non-dimensionalized time by $\delta_i/\Delta U_0$, and the present study also follows this approach. The computational domain is non-dimensionalized by δ_i, the initial vorticity thickness and the Reynolds number based on initial vorticity thickness is 400. The present results are compared to these earlier DNS results. The study by Metcalfe *et al.* used spanwise and streamwise periodic boundary conditions. In the present effort, however, we use periodic boundary conditions only in the streamwise direction and use symmetric conditions in the spanwise direction. This modification was required due to some inherent limitation of the KIVA code. However, this difference is believed to result in negligible effects since the initial fundamental mode disturbance is inherently two-dimensional. It should be noted that the original code can handle axi-symmetric periodic boundary but can not handle periodic boundaries in the streamwise direction, and therefore, minor modifications were implemented in both KIVA-3V and KIVALES so that we can simulate this flow field.

Here, 32^3 and a 64^3 grid simulations were carried out using both KIVALES and LESLIE3D (a fourth-order accurate finite-volume code used extensively in the past[26]). At this particular low Reynolds number and without any random turbulence initialization, the SGS models should not contribute any dissipation. This is confirmed in this study.

Figure 1 shows the growth of fundamental energy mode as a function of time. KIVALES shows a similar trend as in Fig. 1 of Metcalfe *et al.* (1987). Although KIVALES is more dissipative than the DNS or the 4th order LES and eventually is not able to maintain a saturated state of vortex-rollup, the numerical dissipation is significantly reduced (relative to the KIVA-3V code) and shows the correct physical behavior of the vortex rollup. The initial linear energy growth rate $\sigma = (dE/dt)/2E$ predicted by KIVALES is 0.19, which matches to the value of 0.19 predicted by linear instability analysis[23] and predicted by DNS. In contrast, KIVA-3V shows an immediate energy decay right after the initialization, and this is the case even for a higher grid resolution (64^3) case while KIVALES using the higher resolution shows an even better resolution of the fundamental mode energy saturation.

These differences can clearly be seen in the snapshots of the mixing layer at a certain time as shown in Fig. 2. KIVALES shows vortex roll-up at the non-dimensional time of 8 as predicted by DNS and LES (not shown here), and this prediction becomes more accurate as the number of grid points is increased. The "braid" region is more clearly captured in the higher grid resolution case. On the contrary, KIVA-3V shows high dissipation due to turbulence model by a time of 2 even when the higher grid resolution is used. It is clear that the RANS based KIVA-3V code does not simulate vortex rollup correctly.

This study, therefore, shows the importance of numerical and turbulence model dissipation, and its impact in the RANS code. The results demonstrate that the RANS based KIVA-3V is inappropriate to simulate unsteady mixing problem whereas the modified KIVALES resolves energy containing motion.

5.2 Flow over Backward-Facing Step

Even though the simulations of mixing layer yielded a significant difference between KIVALES and the original KIVA-3V, accurate prediction of the evolution of coherent vortices is not sufficient enough to evaluate the effect of turbulence subgrid model. To examine the LES implementation in KIVA code in more detail, flow over a backward-facing step is simulated and the results are compared with the earlier DNS study by Le and Moin[27] and the experiments cited therein.

Computational geometry used in this study is shown in Fig. 3, which is similar to that used by Ak-

selvoll and Moin[28] with the same Expansion Ratio (ER) of 1.2 (also used by Le and Moin for their DNS study). Our geometry incorporates $96 \times 64 \times 32$ in streamwise, wall-normal, and spanwise direction, respectively, which is somewhat finer than the LES of Akselvoll and Moin's study, but this is inevitable due to the lower spatial order of accuracy of KIVA-3V, and subsequently, KIVALES. The geometry incorporates periodic boundary conditions in spanwise direction, and no-slip wall condition is applied to the other boundaries except inlet and outlet. Inlet condition employs a fixed inlet velocity U_0 of 10,000 cm/s with small random fluctuations, and the Reynolds number is 5100 based on the step height.

Figure 4 shows the spanwise- and temporal-averaged spanwise vorticity field. Since RANS solves the time-averaged equations, it is more appropriate to make direct comparison on the averaged quantity rather than the instantaneous quantity. It should be pointed out that there is not much difference between the instantaneous snapshots of KIVA-3V and its temporal averaged snapshots, which is due to the time-averaged nature of the RANS code. The temporal average flow field for the LES is obtained over several flow-through time after around 5 flow-through time after the initialization to obtain statistically stationary state. (1 flow-through time is the total length of geometry divided by inlet mean velocity and represents an approximate travel time for a fluid element to pass through the computational domain.) KIVALES predicts the re-attachment length ($x^R = x/h$) of 6.0, which is also predicted by Le and Moin[27] whereas KIVA-3V predicts an earlier re-attachment length of 4.0. The re-attachment length is calculated from the temporal and spanwise averaged data as the location where the wall-normal velocity gradient is zero. From these snapshots, it also should be realized that KIVALES captures recirculation region clearly, which is characteristic of this type of flow field while KIVA-3V does not.

Mean velocity profile and root mean square streamwise velocity are plotted in Fig. 5. KIVALES follows the earlier DNS study and experimental study reasonably well.

5.3 Internal Combustion Engines

The simulations of mixing layer and backward-facing step have shown that KIVALES has the potential for capturing unsteady flow accurately. Therefore, KIVALES should be able predict more accurately the in-cylinder mixing process. The geometry employed here (Fig. 6) incorporates two moving valves, one of which is used for intake and the other for exhaust. The spray injector is located at the top center of the cylinder. No experimental data for this configuration is currently available but is used here to show that KIVALES is capable of handling more complex engine configurations. Although no combustion is currently investigated it will be the focus of a future study.

As droplet evaporation and subsequent fuel-air mixing process is of interest, we are going to discuss the in-cylinder mixing process with fuel spray here. The geometry used for this study is shown in Fig 6. For comparison purpose, three different fuel injection cases are studied: no injection case, Start-Of-Injection (SOI)=90, and SOI=180 degree Crank Angle (CA). Only SOI=180 case is reported here, although a comparative study of these three cases has been reported elsewhere.[29] In these simulations, the cycle is assumed to be the middle of engine operation at a fixed revolution (1500 RPM). Therefore, initially moderate high temperature (900 K) and some gaseous fuel and combustion products are assumed to remain in the combustion chamber. These conditions are primarily obtained from Han *et al.*[30] Fuel used is gasoline (C_8H_{17}) as a 'single' species and injected directly into combustion chamber in a conical spray, and the spray vaporizes immediately after injection because of the high temperature in the cylinder. The fuel injector is located at the middle of the cylinder top looking vertically downward. Wall boundary condition used is the turbulent 'law-of-the-wall', which is the default KIVA boundary condition. The use of this wall function with LES is still an open question, but it is not feasible to resolve wall layer for in-cylinder turbulent flow with a LES grid. However, its validity might be a topic of future studies using KIVALES.

Shown in Fig. 7 is the comparison between KIVALES and KIVA-3V of the droplet 'parcels' inside the cylinder and the stoichiometric surface due to spray evaporation at 90 degrees after SOI. Obviously, KIVALES shows a more wrinkled stoichiometric surface due to the resolved scale turbulent motion. This effect can also be seen in Fig. 8, in which the spatially averaged modeled-part turbulent kinetic energy is plotted. Obviously, KIVA-3V shows a larger value of the turbulent kinetic energy than KIVALES. This is understandable since in the LES, the subgrid kinetic energy represents only the energy unresolved on the grid whereas in the RANS approach, all turbulent kinetic energy is considered unresolved and hence, modeled.

Particle dispersion by turbulence is studied both numerically and experimentally.[31–33] In this study, we study particle dispersion in terms of the second invariance of deformation tensor following Hunt *et*

al.[34] The second invariant of deformation tensor is defined as

$$II_d = \frac{\partial u_i}{\partial x_j}\frac{\partial u_j}{\partial x_i} = S_{ij}S_{ji} + R_{ij}R_{ji} = S_{ij}S_{ij} - \frac{1}{2}\omega_i\omega_i \tag{18}$$

Squires and Eaton[35,36] have found this quantity and the particle concentration are weakly correlated, and, on the other hand, the invariant and enstrophy is negatively correlated. It can be intuitively understood that since droplets have higher density than the surrounding liquid, droplet particles are more and more pushed outward by the centrifugal force in strongly rotating region. The evolution of the number density of particles in terms of the invariant is shown in Fig. 9. The distribution is widely spread for both positive and negative value at the early CA after SOI, however, the distribution evolves with CA and shows a strong preference at CA of 260. This tendency is not confirmed by KIVA-3V, which lacks the ability to capture shear regions and vortical structures. Our correlation with KIVALES is still very weak, and this is probably because particle response time is much larger than the characteristic flow time, which is the engine piston speed in IC engine case. It is interesting to note that positive correlation between the invariant and particle concentration occurs even in a relatively short time. However, the effects of droplet evaporation cannot be determined from this data.

Another interesting observation is that KIVA-3V, KIVALES, and KIVALES-LEM all predicts nearly same spatial mean evaporated fuel mass fraction profile. However, KIVALES-LEM predicts larger scalar variance compared to the other two code (Fig. 10). This would be the consequence of subgrid turbulent motion. It is interesting to mention that, at each CA, KIVALES and KIVALES-LEM showed qualitatively almost similar scalar distribution in the cylinder. However, it is known that the conventional gradient-diffusion closure fails in reactive flow field,[37] therefore, these two closures should be compared in a reactive flow field. Our future study will address this issue. As piston approaches TDC and turbulence decays, the three curves converge close to each other, however, the actual PDF of fuel mass fraction is different in each case (not shown here).

6 Conclusion

The new KIVA code with LES capability has been validated using several different flow fields, and in every study, the LES version of KIVA code yielded promising results. In contrast, the original KIVA-3V code completely failed to predict the unsteady turbulent flows. It is clear from the present study that in order to capture the dynamics of in-cylinder anisotropic turbulent mixing LES appears to be the only feasible approach. However, there are several issues that remain to be resolved. For example, although the subgrid scalar mixing model based on LEM has shown significant promise in earlier LES studies, the applicability of LEM in the study of IC engine fuel-air mixing flows remains to be established. In particular, in the direct injection spark ignition type engine different combustion regimes (non-premixed, premixed and partially premixed) occurs depending upon the engine operation condition and for this type of flow, the LEM subgrid scalar mixing model may prove to be particularly useful. Another unresolved issue is the application of the wall boundary condition. Currently, a law-of-the-wall condition as in the original KIVA is employed. However, wall boundary condition is of particular importance in the LES of wall-bounded flows and therefore, its effect will have to be investigated. Finally, for practical application to realistic engines, chemical reactions and effect of heat release has to be studied. Again, for such studies, the subgrid LEM provides an unique capability to close the reaction rate in an exact manner and may prove to be a viable SGS approach. These issues will be addressed in the near future.

7 Acknowledgment

We thank Ford Motor Company for their support and acknowledge additional support by a Connectivity Grant from Engineering Research Center at Mississippi State University.

A Filtered Specific Internal Energy Equation

The total energy equation of gas phase for reacting compressible flow with spray is[38]

$$\frac{\partial \rho E}{\partial t} + \frac{\partial}{\partial x_j}\left(\rho E u_j + q_j - u_i\tau_{ij}\right) = \dot{Q}^{spray}, \tag{19}$$

in which internal energy is defined as $e = h - p/\rho$, where $h = \sum_m Y_m(\Delta h^0_{f,m} + \int_{T_{ref}}^{T} C_{p,m}dT')$.

Subtracting kinetic energy contributions (Using momentum equation given as Eqn.(2)) from the total energy equation, yields the following internal energy equation:

$$\frac{\partial \rho e}{\partial t} + \frac{\partial \rho u_j e}{\partial x_j} = -\frac{\partial q_j}{\partial x_j} + \tau_{ij}\frac{\partial u_i}{\partial x_j} + \dot{Q}^{spray} - F^s_i u_i. \tag{20}$$

The last two terms represent spray effects and denoted as $\dot{Q}^s$.

Filter equation (20) to obtain specific internal energy equation for LES (3):

$$\frac{\partial \bar{\rho}\widetilde{e}}{\partial t} + \frac{\partial}{\partial x_j}\left(\bar{\rho}\tilde{u}_j\tilde{e} + \bar{q}_j + h_j^{sgs}\right)$$
$$= -\bar{p}\frac{\partial \tilde{u}_j}{\partial x_j} + \overline{\sigma}_{ij}\frac{\partial \widetilde{u_i}}{\partial x_j} + \Theta^{sgs} + \Pi^{sgs} + \overline{\dot{Q}^s}$$

where $h_j^{sgs} = \bar{\rho}(\widetilde{eu_j} - \tilde{e}\tilde{u}_j) + \overline{pu}_j - \bar{p}\tilde{u}_j$, $\Pi^{sgs} = \overline{u_j\frac{\partial p}{\partial x_j}} - \tilde{u}_j\frac{\partial \bar{p}}{\partial x_j}$, and $\Theta^{sgs} = \overline{\sigma_{ij}\frac{\partial u_i}{\partial x_j}} - \overline{\sigma_{ij}}\frac{\partial \tilde{u}_i}{\partial x_j}$. Note that stress tensor is decomposed into pressure work and viscous work.

It should be pointed out that chemical source term $\dot{Q}^c$ in the original equation[14] is included in our definition of internal energy.

References

[1] Anderson, R. W., Yang, J., Brehob, D. D., Vallance, J. K., and Whiteaker, R. M. Understanding the Thermodynamics of Direct Injection Spark Ignition (DISI) Combustion Systems: An Analytical and Experimental Investigation. SAE Paper, 962018, 1996.

[2] Kume, T., Iwamoto, Y., Iida, K., Murakami, M., Akishino, K., and Ando, H. Combustion Control Technologies for Direct Injection SI Engine. SAE Paper, 960600, 1996.

[3] Zhao, F., Lai, M.-C., and Harrington, D. L. Automotive spark-ignited direct-injection gasoline engines. *Progress in Energy and Combustion Science*, 25:437– 562, 1999.

[4] Amsden, A. A. KIVA-3V: A Block-Structured KIVA Program for Engines with Vertical or Canted Valves. Technical Report LA–13313–MS, Los Alamos National Laboratory, July 1997.

[5] Heywood, J. B. *Internal Combustion Engine Fundamentals*. McGraw-Hill Inc., 1988.

[6] Galperin, B. and Orszag, S., editors. *Large Eddy Simulation of Complex Engineering and Geophysical Flows*. Cambridge University Press, 1993.

[7] Naitoh, K., Itoh, T., Takagi, Y., and Kuwahara, K. Large Eddy Simulation of Premixed-Flame in Engine based on the Multi-Level Formulation and the Renormalization Group Theory. SAE Paper, 920590, 1992.

[8] Haworth, D. C. Large Eddy Simulation of In-Cylinder Flows. In *International Conference on Multi-dimensional Simulation Simulation of Engine Internal Flows*, Rueil-Malmaison, France, Dec. 3-4 1998. IFP.

[9] Haworth, D. C. and Jansen, K. Large-eddy simulation on unstructured deforming meshes: towards reciprocating IC engines. *Computers and Fluids*, 29:493–524, 2000.

[10] Celik, I., Yavuz, I., Smirnov, A., Smith, J., Amin, E., and Gel, A. Prediction of In-Cylinder Turbulence for IC Engines. *Combustion Science and Technology*, 153:339–368, 2000.

[11] Menon, S., Yeung, P.-K., and Kim, W.-W. Effect of Subgrid Models on the Computed Interscale Energy Transfer in Isotropic Turbulence. *Computers and Fluids*, 25(2):165–180, 1996.

[12] Kerstein, A. R. Linear-Eddy Modelling of Turbulent Transport. Part 6. Microstructure of Diffusive Scalar Mixing Fields. *Journal of Fluid Mechanics*, 231:361–394, 1991.

[13] Menon, S., McMurtry, P.A., and Kerstein, A. R. A Linear Eddy Mixing Model for Large Eddy Simulation of Turbulent Combustion. In Galperin, B. and Orszag, S., editors, *Large Eddy Simulation of Complex Engineering and Geophysical Flows*. Cambridge University Press, 1993.

[14] Amsden, A. A., O'Rourke, P. J., and Butler, T. D. KIVA-II: A Computer Program for Chemically Reactive Flows with Sprays. Technical Report LA–11560–MS, Los Alamos National Laboratory, May 1989.

[15] Chakravarthy, V. K. and Menon, S. Large-Eddy Simulations of Turbulent Premixed Flames in the Flamelet Regime. *Combustion Science and Technology*, 2000. (to appear).

[16] Kim, W.-W. and Menon, S. LES of Turbulent Fuel-Air Mixing in a Swirling Combustor. AIAA Paper, 98-0200, 1998.

[17] Kim, W.-W., Menon, S., and Mongia, H. C. Large Eddy Simulations of Reacting Flow in a Dump Combustor. AIAA Paper, 98-2432, 1998.

[18] Calhoon, W. H. and Menon, S. Subgrid Modeling for Reacting Large Eddy Simulations. AIAA Paper, 96-0516, 1996.

[19] Stone, C. and Menon, S. Simulation of Fuel-Air Mixing and Combustion in a Trapped-Vortex Combustor. AIAA Paper, 2000-0478, 2000.

[20] Sone, K. and Menon, S. Implementation of Large-Eddy Simulation into the KIVA code. Part 1. Evaluation of KIVALES. Technical Report CCL-2001-008, Georgia Institute of Technology, 2000.

[21] Chakravarthy, V. K. and Menon, S. Subgrid Modeling of Premixed Flames in the Flamelet Regime. *Flow, Turbulence and Combustion*, 2000. (to appear).

[22] Pannala, S. *On Large eddy Simulations of Reacting Two-Phase Flows.* PhD thesis, Georgia Institute of Technology, Atlanta, GA, May 2000.

[23] Michalke, A. On the Inviscid Instability of the Hyperbolic-tangent Velocity Profile. *Journal of Fluid Mechanics*, 19:543–556, 1964.

[24] Metcalfe, R. W., Orszag, S. A., Brachet, M. E., Menon, S., and Riley, J. J. Secondary Instability of a Temporally Growing Mixing Layer. *Journal of Fluid Mechanics*, 184:207–243, 1987.

[25] Riley, J. J. and Metcalfe, R. W. Direct Numerical simulation of a Perturbed, Turbulent Mixing Layer. AIAA Paper, 80-0274, 1980.

[26] Nelson, C. and Menon, S. Unsteady Simulations of Compressible Spatial Mixing Layers. AIAA Paper, 98-0786, 1998.

[27] Le, H. and Moin, P. Direct Numerical Simulation of Turbulent Flow over a Backward-Facing Step. *CTR Annual Research Briefs*, pages 161–173, 1992.

[28] Akselvoll, K. and Moin, P. Large Eddy Simulation of Turbulent Confined Coannular Jets and Turbulent Flow Over a Backward Facing Step. Technical Report TF-63, Stanford University, 1995.

[29] Sone, K. and Menon, S. The Effect of Subgrid Modeling on the In-Cylinder Unsteady Mixing Process in a Direct Injection Engine. *Manuscript submitted to the ASME Spring Technical Conference*, 2001.

[30] Han, Z. and Reitz, R. D. Turbulence Modeling of Internal Combustion Engines Using RNG $k-\varepsilon$ Models. *Combustion Science and Technology*, 106:267–295, 1995.

[31] Kobayashi, H., Masutani, S. M., Azuhata, S., and Arashi, N. Dispersed Phase Transport in a Plane Mixing Layer. In Hirata, M. and Kasagi, N., editors, *Transport phenomena in turbulent flows*, pages 433–466. Hemisphere Publishing Corporation, 1988.

[32] Longmire, E. K. and Eaton, J. K. Structure and Control of a Particle-Laden Round Jet. In *Fluids Engineering: Korea - U.S.Progress*, pages 465–484. Hemisphere Publishing Corporation, 1989.

[33] Elghobashi, S. and Truesdell, G. C. On the two-way interaction between bomogeneous turbulence and dispersed solid particles. I. Turbulence modification. *Physics of Fluids A*, 5(7):1790–1801, 1993.

[34] Hunt, J. C. R., Wray, A. A., and Moin, P. Eddies, Streams, and Convergence Zones in Turbulent Flows. *Center for Turbulence Research Proceedings of the Summer Program*, pages 193–208, 1988.

[35] Squires, K. D. and Eaton, J. K. Particle response and turbulence modification in isotropic turbulence. *Physics of Fluids A*, 2(7):1191–1203, 1990.

[36] Squires, K. D. and Eaton, J. K. Preferential concentration of particles by turbulence. *Physics of Fluids A*, 3(5):1169–1178, 1991.

[37] Pope, S. B. The Statistical Theory of Turbulent Flames. *Philosophical Transactions of the Royal Society of London*, 291:529–568, 1979.

[38] Oefelein, J. C. and Yang, V. Analysis of Transcritical Spray Phenomena in Turbulent Mixing Layers. AIAA Paper, 96-0085, 1996.

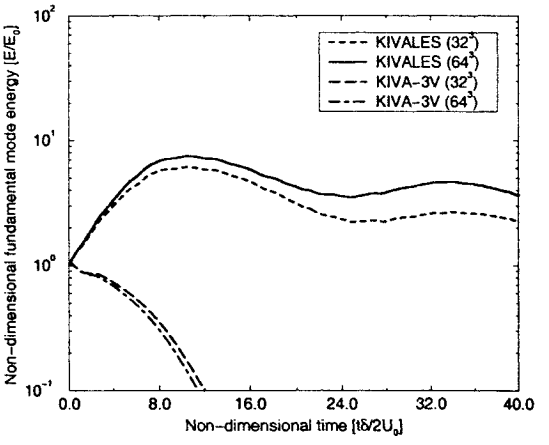

Fig. 1 Resolved scale fundamental mode energy growth. The linear growth rate of KIVALES is 0.19, which is also predicted by Michalke.[23] In contrast, KIVA-3V rapidly dissipates the energy.

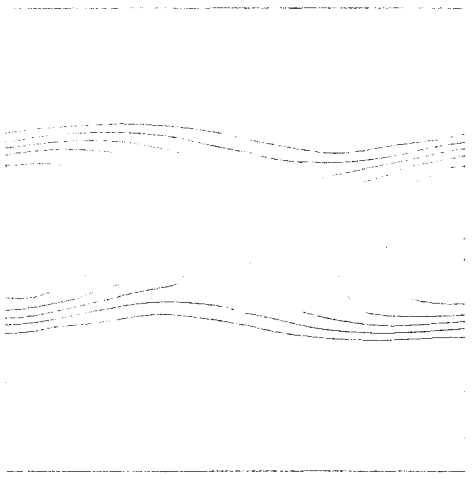

a) KIVA-3V at $\mathcal{T} = 2$

b) KIVALES at $\mathcal{T} = 8$

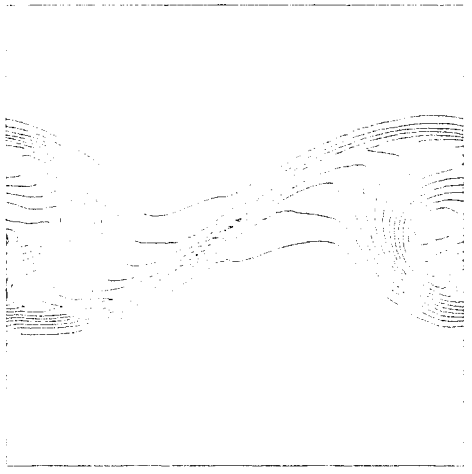

c) KIVALES at $\mathcal{T} = 8$ with 64^3 grid

Fig. 2 Spanwise vorticity field in the temporal mixing layer. The figures are drawn using the same contour interval of $\Delta\omega = 500(sec^{-1})$.

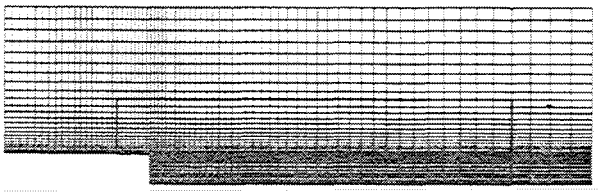

Fig. 3 Geometry used for the simulation of flow over backward-facing step. Number of cells is $96 \times 64 \times 32$. Only an area closed by a bold line is shown in the next figure.

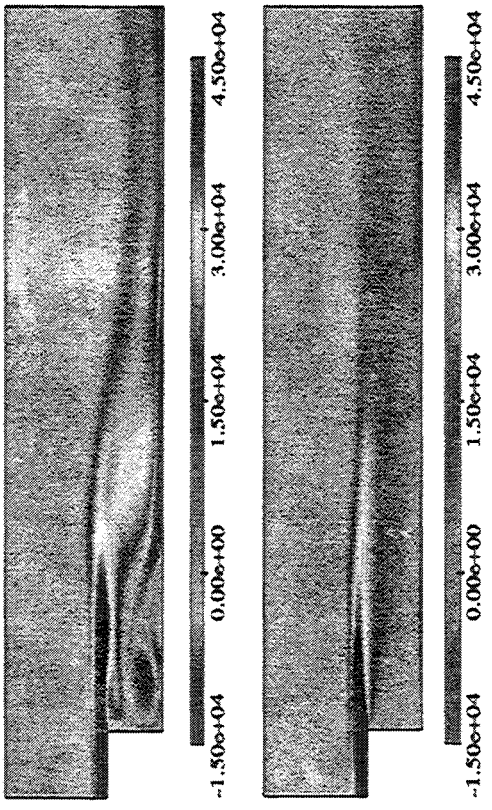

a) KIVALES b) KIVA-3V

Fig. 4 Spanwise and temporal averaged spanwise vorticity.

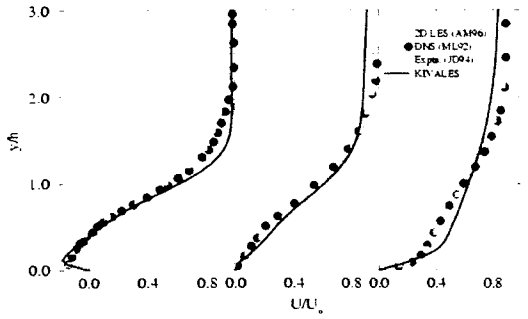

a) $\overline{U}$

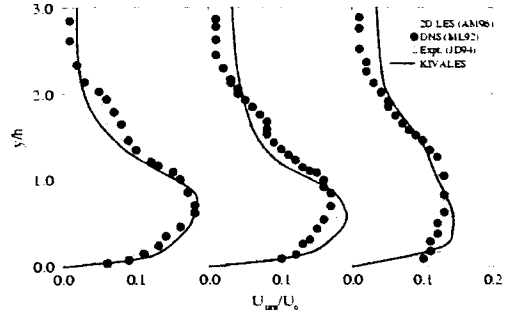

b) u^{rms}

Fig. 5 Spanwise and temporal averaged mean streamwise-velocity and root mean square streamwise-velocity

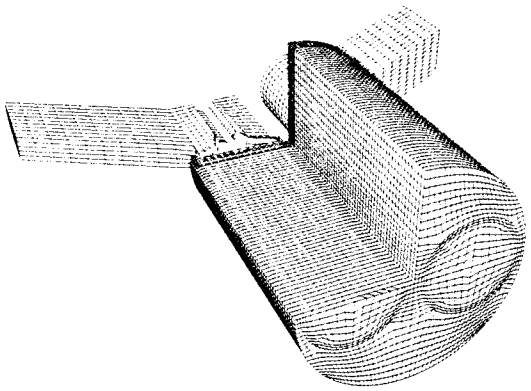

Fig. 6 Geometry used for the simulations of IC engine. It incorporates around 80,000 cells at BDC.

a) KIVALES

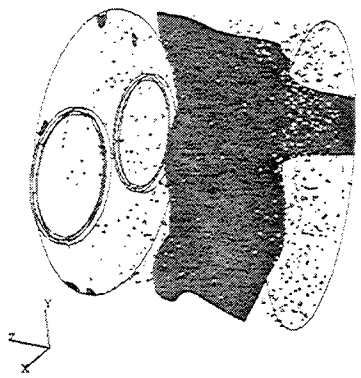

b) KIVA-3V

Fig. 7 Stoichiometric surface at CA=270, which is 90 degrees after SOI.

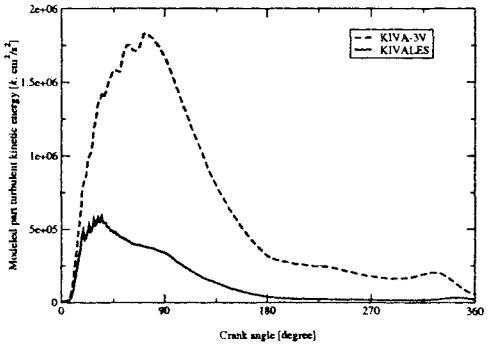

Fig. 8 Comparison between the turbulent kinetic energy of KIVA-3V and SGS turbulent kinetic energy of KIVALES. Both of them show the modeled turbulent energy, and the former is significantly larger than the latter.

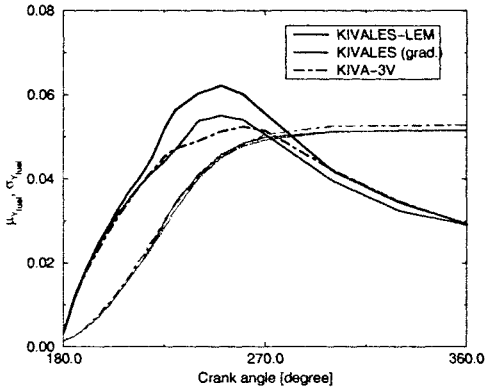

Fig. 10 Temporal evolution of scalar (fuel mass fraction) mean (μ) and variance (σ^2) (standard deviation (σ) is shown) for comparison between gradient diffusion closure KIVALES and KIVALES-LEM. Light lines denote mean while black lines denote standard deviation. Note that LEM predicts larger scalar variance between BDC and TDC.

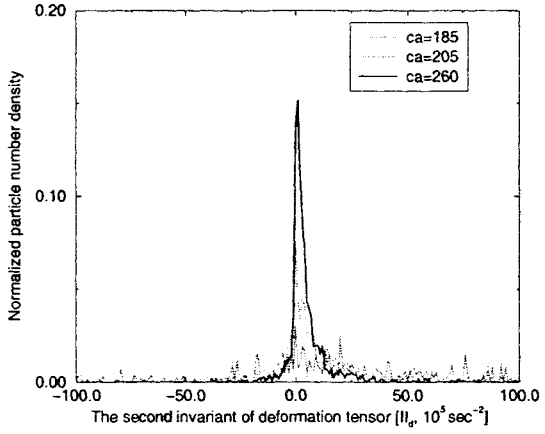

Fig. 9 Correlation between the second invariant of deformation tensor and particle concentration.